Computational fluid dynamic modeling of gas flow characteristics of the high-power CW CO_2 laser

Hongyan Huang (黄鸿雁) and Youqing Wang (王又青)*

Wuhan National Laboratory for Optoelectronics, School of Optoelectronic Science and Engineering, Huazhong University of Science and Technology, Wuhan 430074, China

**Corresponding author: yqwang13@163.com*

Received June 12, 2010; accepted July 10, 2010; posted online January 1, 2011

To increase the photoelectronic conversion efficiency of the single discharge tube and to meet the requirements of the laser cutting system, optimization of the discharge tube structure and gas flow field is necessary. We present a computational fluid dynamic model to predict the gas flow characteristics of high-power fast-axial flow CO_2 laser. A set of differential equations is used to describe the operation of the laser. Gas flow characteristics, are calculated. The effects of gas velocity and turbulence intensity on discharge stability are studied. Computational results are compared with experimental values, and a good agreement is observed. The method presented and the results obtained can make the design process more efficient.

OCIS codes: 000.4430, 140.3425, 140.3470.
doi: 10.3788/COL201109.011401.

High-power fast-axial flow (FAF) CO_2 laser is a well-established cutting tool in the manufacturing industry. In large-format laser cutting systems, the laser generally moves with the whole system along the guide rail; therefore, the structure of the laser has to be as compact and light as possible. The key factor in achieving all these characteristics is to raise the photo electronic conversion efficiency of the single discharge tube. This technology has been under continuous improvement. In the early stage, a single discharge tube of cruciform structure can reach a maximum output of merely 290 W with an optimized entrance nozzle structure. A maximum output of 333 W can be achieved. We recently discovered that the maximum output power of the single discharge tube can reach 500 W. The core theory of this progress is the discharge tube structure and the gas flow field optimization. However, there has been very little domestic research on this subject.

Many studies on FAF CO_2 lasers have focused on the modeling of laser processes in the laser medium[1−9]. The effects of turbulence flow on the performance of the FAF CO_2 laser have also been discussed[10−13]. These studies have provided good theoretical bases for our research. Computational fluid dynamic (CFD) method has become a powerful approach to analyze the three-dimensional (3D) flow in complicated domains. We can make use of previous researches and the CFD method to obtain further insight on the realistic gas flow of the laser and make the design more efficient.

In our earlier letter[14], we presented a preliminary attempt on numerical investigation of a FAF CO_2 laser using CFD method, and the results were encouraging. However, much improvement is needed before the actual application. Our previous work simplified the discharge cavity into a straight tube. With the further demand for laser researches and a more accurate grasp of the internal flow field, we established a realistic 3D discharge tube model, including the turbulence generator and the anode and cathode area. In our previous work, the effect of the external electric field was only described via a given constant value, which was equal to the difference between the input electric and laser output power. This approach was not sufficiently accurate because the electric field effects on particular regions inside the laser cavity are different. The contribution of electrons of vibrational states and relaxation of electrons from the asymmetric stretch vibrational levels of CO_2 to the ground level also need to be considered[15]. In this letter, we divide the computational grid into four regions, and then set the source term.

An overall view of the grids used in the computations is shown in Fig. 1. The size of the grid is approximately 129184 cells. From Fig. 1, the turbulence generator is constituted by a cylindrical annular cavity located outside the ellipsoid chamber with a gas inflow opening. The jet orifice connecting the cylindrical annular cavity and ellipsoid chamber is opposite the initial gas inlet and 45° away from the axial. The electrode pin is coaxially disposed with the axis of the jet orifice. This structure helps generate a vortex street and a high-turbulence gas flow, according to the following numerical investigations.

The model consists of a set of differential equations for numerical solution of discharge process of the FAF CO_2 laser. Before introducing the governing equations, we discuss the division of the computational grids, which is the main improvement from our previous work. The gases in the region of fluid inlet and the cylindrical annular cavity have not been excited; in other words, the effect of the electric field and electric current need not take the energy conservation equation into account. We define this region as inflow area. The region of intense electrical heating near anode pin is the ellipsoid chamber. We define this region as the anode area. The region inside the cylinder of the radius 19.15 mm between the axial distances of 20.42 and 216.3 mm is defined as the positive column area. The axial distance between 216.3 and 224.3 mm is defined as the cathode area. The related source terms will be set

into the four areas.

CFD method is the numerical simulation of flow under the control of the basic flow equation (conservation of mass, momentum, and energy equations). In this letter, the conservation equations of mass and momentum for the gas flow in the discharge tube are the same as the non-ionized gas if the contribution of the electric force is ignored. However, the energy equation should consider the contribution of electron of vibrational states, relaxation of electrons from the asymmetric stretch vibrational levels of CO_2 to the ground level, and electrical heating. We are interested in the small-signal gain; therefore, the intensity I_v inside the cavity is assumed to be 0. The distributions of the internal flow fields in the discharge tube are considered as in steady-state; thus, we can neglect time-term in governing equations. The governing equations of the dynamic process in the laser cavity can be written as[5,6,8]

$$\frac{\partial \rho u_i}{\partial x_i} = 0, \tag{1}$$

$$\frac{\partial \rho u_i u_j}{\partial x_j} = -\frac{\partial p}{\partial x_i} - \frac{f}{2d_r}\rho u^2, \tag{2}$$

$$\begin{aligned}\frac{\partial \rho u_j h_{\mathrm{B}}}{\partial x_i} = {} & \frac{\partial}{\partial x_i}\left(\Gamma \frac{\partial h_{\mathrm{B}}}{\partial x_i}\right) + \frac{\partial p}{\partial t} + u_i \frac{\partial P}{\partial x_i} + \bar{\tau}_{ij}\frac{\partial u_i}{\partial x_j} \\ & - n_{\mathrm{e}} h (n_{\mathrm{co_2}} v_3 \chi_3 + n_{\mathrm{N_2}} v_4 \chi_4) \\ & + \frac{\rho[h_3 - h_3(T)]}{\tau_3} + IE, \end{aligned} \tag{3}$$

where ρ is the gas density; u_i are the components of the gas velocity (i=x, y, z); x_i are the space coordinates; P is the gas pressure; f=$0.3164Re^{-1/4}$ is the friction coefficient, where $Re = (\rho u/\mu)d_r$ is the Reynolds number, μ is the viscosity of the gas, and d_r is the discharge tube diameter[4]; Γ is the diffusion coefficient, which will be defined and discussed later; $\bar{\tau}_{ij}$ are the elements of the stress tensor; n_{e} is the electron density; h is the value of the Planck constant; $n_{\mathrm{CO_2}}$ and $n_{\mathrm{N_2}}$ are the concentrations of the molecules of CO_2 and N_2; v_3 and v_4 are the frequency of the first excited state of the asymmetrical stretch mode and frequency spacing between the N_2 vibrational levels; χ_3 and χ_4 are the excitation rates of the asymmetric stretch mode of CO_2 and of the vibrational mode of N_2, respectively; h_3 is the specific vibrational energy of the asymmetric stretch mode of CO_2 (we assume that the stimulated emission occurs only for 10P (20) transitions in the (00^01, J) → (10^00, J+1) band); τ_3 is the relaxation time of energy transfer from the CO_2 asymmetric mode to the combined CO_2 bending and symmetric stretch mode; I is the electric current, E is the electric field intensity, and IE is the electrical heating of the gas[5,8].

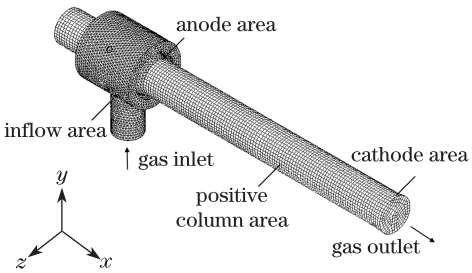

Fig. 1. General view of the grids used in our computations.

Table 1. Initial Input Parameters of the Computational Model

Mixing Gas	Notation	Value
Tube Length	L (mm)	274.1
Tube Diameter	D (mm)	19.15
Average Molecular Weight	M (kg/mol)	12.28
Thermal Conductivity	k [W/(m· K)]	0.0943
Viscosity	μ [kg/(m· s)]	2.313×10^{-5}
Heat Capacity at Constant Pressure	c_{p} [J/(kg·K)]	1943
Inlet Gas Pressure	P (Pa)	18400
Outlet Gas Pressure	P (Pa)	10400
Inlet Gas Temperature	T_{i} (K)	293
Outlet Gas Temperature	T_{o} (K)	421

After the computational grids have been established and the conservation equations of mass, momentum, and energy have been presented and discussed, the next step is to import the grid into FLUENT software. FLUENT software only contains the basic flow equations; therefore, the contribution of the electric field effect added in the energy equation will be loaded as user-defined functions according to the write programs. The CFD-solving process in FLUENT software has been shown in our earlier letter[14].

The boundary and initial conditions are key parts of the computational procedure because they are the prerequisites of the correct solutions of the governing equations. For the compressible turbulent flow model, the gas inlet and gas outlet adopted the pressure inlet and the pressure outlet boundary conditions, respectively. The initial conditions included the gas inlet and outlet pressure, temperature, and many other dynamic parameters. The inlet temperature was assumed to be equal to room temperature 293 K. The outlet temperature was 421 K, which was measured in the experiment. Therefore, the qualitative temperature which was the mean value of the inlet and outlet temperatures was expected to be 357 K. This temperature was used for the estimation of the material parameters, which had to be defined before starting iteration[18]. The input parameters of the model are shown in Table 1.

As shown in Figs. 2 and 3, the gas pressure and density of the laser cavity are calculated versus tube length at 3 mm (plots A) away from the central longitudinal line of the laser cavity, the center line (plots B), and at –3 mm (plots C) away from the center line. Since the inlet opening is located at 51-mm radius from the laser axis, the pressure and density variation in the region of the inflow area cannot be presented in the two figures. However, the positive column region is the main part that reflects the discharge process in the laser cavity. There-

fore, we select the three given lines as representative explanations. The zero-point in the x-axis is opposite the center of the jet orifice connecting the cylindrical annular cavity and ellipsoid chamber. Apart from the small region near the entrance of the tube, the gas pressure and density variations do not exceed 10%, and are only slightly dependent on the distance from the axis. At the fore part, the significant decrease is mainly due to the gas mixture introduced in the tube through the narrow orifice to the ellipsoid chamber. The dimension of the flow section suddenly increases. This is related to the decrease of the radius of the laser cavity.

The gas velocity nephogram in the central longitudinal section of the laser cavity is shown in Fig. 4. Since the anode pin is placed opposite the initial gas inlet and 45° away from the axial, the anode pin and jet orifice cannotbe seen in this figure. According to the fluid dynamic theory, the input flow blows through the narrow orifiyce with a cross-section several times smaller than that of the discharge tube. Thus, the input gas flow is near-sonic, highly turbulent, and has a distinct turbulent core near the entrance. The computational result shown in Fig. 4 justifies the above analyses. The turbulent core is in the center of the ellipsoid chamber. The distributions of the gas velocity in the inflow and anode regions

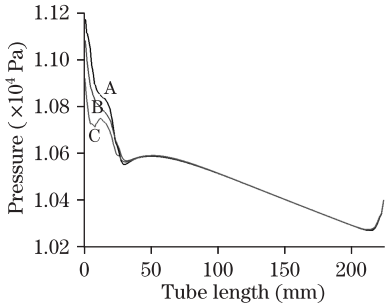

Fig. 2. Plots of the gas pressure versus tube length at 3-mm radial distance (curve A), at the center line (curve B), and at –3-mm radial distance (curve C) of the discharge tube.

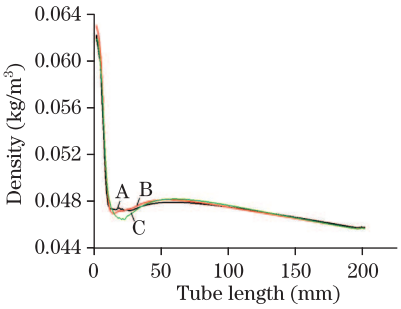

Fig. 3. Gas density versus tube length.

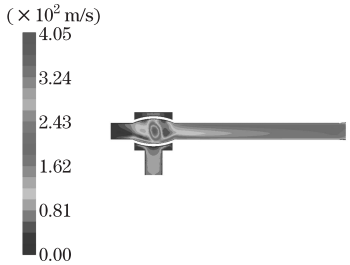

Fig. 4. Contours of velocity distribution inside the laser cavity.

are non-uniform because of the high turbulent from the cylindrical annular cavity and nozzle. The above distributions are not shown in our previous work. After the anode region, the gas velocity and its distribution stability increase along the discharge tube length, especially downstream of the positive column region, which is the main area determining discharge stability. This is the global distribution showing the overall distribution trends of the gas velocity. To obtain the detailed distribution of the gas velocity, the following analysis is needed.

The plots of the axial velocity versus axial length under the inlet openings are shown in Fig. 5. The selection of the curves is similar to that in Fig. 2. From Fig. 5, the largest axial velocity is at the zero-point, which is the center of the nozzle. The sharp drop after the zero-point is due to the introduction of the gas mixture in the tube through the narrow orifice to the ellipsoid chamber and the sudden increase in the dimension of the flow section. The initial increase after the sharp drop of this velocity is related to the decrease of the radius of the laser cavity. The increase is related to the decrease of the plasma density (see Fig. 3) which is caused by the increase of the temperature heated by the gas discharge. The decrease beyond the cathode is related to the increase of the radius of the laser cavity. In the region of 25–220 mm, the increase of gas velocity is nearly linear, and the differences among curves A, B, and C are negligible. Therefore, the gas velocity distribution is uniform.

Previous studies have demonstrated that high velocity is helpful in the timely removal of the heat from discharge and in obtaining high efficiency. However, in the optimization process, even if the gas velocity is high, the gas discharge appears jittery, and the electrical power cannot be injected when the excitation current increases to a certain extent. The unreasonably designed discharge tubes cannot obtain uniform distribution of the gas velocity. Therefore, the uniform distribution of gas velocity is an important prerequisite for increasing the output power.

The effect of gas flow turbulence on laser output has been investigated in the previous research; results showed that gas flow turbulence was important for increasing laser power[4]. However, a highly turbulent flow also means a large instability factor in the gas flow. Moreover, an unstable distribution of the turbulent intensity will cause severe local heating of the gas, with increase in current intensity. This makes the light area constrict to the tube center where the turbulent intensity is weak, and causes the necking phenomenon of the plasma. Therefore, a stable distribution of turbulent intensity at the discharge tube center is an important prerequisite for a uniform and stable glow discharge. The turbulent intensity distributions need to be calculated and displayed. Figure 6 shows the turbulence intensity versus the tube diameter at 50 mm (curve A), 100 mm (curve B), and 150 mm (curve C) away from the initial gas inlet of the laser tube. From this figure, near the entry of the laser cavity, the highly turbulent flow is generated by the entrance structure to increase the probability of particles collision. The turbulent intensity is high, but unstable. When the gas flow tends towards stability along the tube length, the turbulence intensity also tends to stabilize.

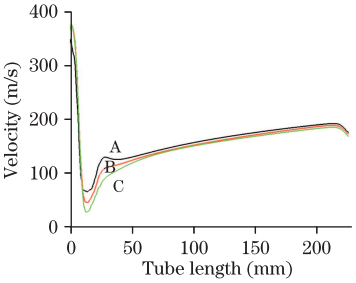

Fig. 5. Gas velocity versus tube length.

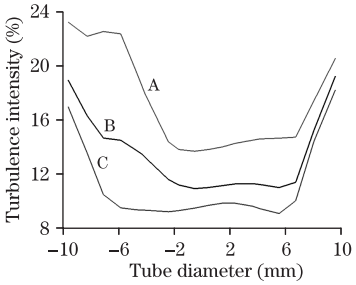

Fig. 6. Plots of the turbulence intensity versus tube diameter at 50 (curve A), 100 (curve B), and 150 mm (curve C) axial length of the discharge tube.

The turbulence intensity decreases along the tube length; however, the stability increases. At 150 mm away from the initial gas inlet, the distribution of the turbulence intensity is nearly symmetrical, and the value change is minimal in the region of –6–6 mm, which represents that the distribution of turbulence intensity is nearly stable in the tube center.

Our experiments were carried out on a DC-excited FAF CO_2 laser developed in our institute using nominal output power of 4 kW. Actual measurement of the internal flow field of the laser cavity is difficult; thus, we determined its dimension by observing whether there was discharge channel jitter with the increase in excitation current. Discharge tubes with external circumferential flow structure were applied in the laser. The excitation current then gradually increased to observe the discharge process under different injection electric powers. The tube can maintain a stable glow discharge when the excitation current increased from 45 to 85 mA. According to the observation, the gas flow pattern is as stable as the computation results (Figs. 5 and 6).

Comparison of the computational results and the experimental value of the gas flow characteristics are given in Table 2. There is a good agreement between the computation and experiment. Although slight differences exist, results are not affected.

In conclusion, the turbulence flow in the optimized discharge tube has been numerically investigated by CFD method to provide a simulation and optimum design criteria for high-power FAF CO_2 laser. The complete structure 3D model and the partial loading source terms have allowed us to describe more accurate details of the internal gas flow field distribution. Results have shown that uniform axial gas velocity and stable radial turbulence are necessary to ensure a uniform and stable glow discharge, which is an important prerequisite in increasing the photoelectronic conversion efficiency of the single discharge tube. Results of computations have been shown to be in reasonable agreement with the experimental observations.

Table 2. Computational Results and Experimental Values of the Gas Flow Characteristics

Gas Flow Characteristics	Computational Results	Experimental Values
Inlet Mass Flow-Rate (kg/s)	0.00279	0.00285
Outlet Temperature (K)	430	421
Pressure Loss (Pa)	796	800
Output Power (W)	330.8	333.3

In the initial design development stage, errors will be discovered, and design changes will be required. According to the approach presented in this letter, we can predict the gas flow field of the initially designed discharge tube via the computer. This has been proven to be an effective method to make the design process more efficient.

This work was supported by the National Key Technology Research and Development Program under Grant No. 2007BAF11B01.

References

1. R. E. Beverly, Opt. Quantum Electron. **14,** 25 (1982).
2. S. Muller and J. Uhlenbusch, J. Phys. D: Appl. Phys. **20,** 697 (1987).
3. M. G. Baeva and P. A. Atanasov, J. Phys. D: Appl. Phys. **26,** 546 (1993).
4. R. Rudolph, A. Harendt, P. Bisin, and H. Gundel, J. Appl. Phys. **26,** 552 (1993).
5. S. Sazhin, P. Wild, C. Leys, D. Toebaert, and E. Sazhina, J. Appl. Phys. **26,** 1872 (1993).
6. S. Sazhin, P. Wild, F. Sazhin, D. Toebaert, and E. Sazhina, J. Phys. D: Appl. Phys. **27,** 464 (1994).
7. S. Al-Hawat and K. Al-Mutaib, Opt. Laser Technol. **39,** 610 (2007).
8. S. Jelvani and H. Saeedi, Opt. Laser Technol. **40,** 459 (2008).
9. S. Sazhin, P. Wild, D. E. Sazhina, M. Makhlouf, C. Leys, and D. Toebaert, Opt. Laser Technol. **26,** 191 (1994).
10. W. J. Wiegand and W. L. Nighan, Appl. Phys. Lett. **26,** 554 (1975).
11. S. A. Buyarov, V. D. Dubrov, M. G. Galushkin, V. S. Golubev, R. V. Grishayev, A. A. Ionin, A. A. Kotkov, V. Y. Panchenko, and Y. N. Zavalov, in *Proceedings of Seventh International Conference on Laser and Laser-Information Technologies* 176 (2001).
12. M. G. Galushkin, V. S. Golubev, Yu. N. Zavalov, V. D. Dubrov, R. V. Grishaev, and S. A. Buyarov, in *Proceedings of XV International Symposium on Gas Flow, Chemical Lasers, and High-Power Lasers* 469 (2004).
13. G. Vlad, O. Boiron, G. Paleec, and P. Bournot, in *Proceedings of Gas Flow and Chemical Lasers: Tenth International Symposium* 565 (1994).
14. Q. Li and Y. Wang, Chin. Opt. Lett. **6,** 513 (2008).
15. V. V. Nevdakh, Proc. SPIE **6731,** 67311F (2007).
16. M. Qiu, J. Hu, and Z. Yao, Chinese J. Lasers (in Chinese) **36,** 1296 (2009).
17. H. Ruan, J. Lu, B. Yang, X. Wang, and H. Liu, Chinese J. Lasers (in Chinese) **36,** 1233 (2009).
18. P. Lu and R. Wang, Chinese J. Lasers (in Chinese) **28,** 775 (2001).